

Levy, D.A., Zuza, A.V., Haproff, P.J., and Odlum, M.L., 2020, Early Permian tectonic evolution of the Last Chance thrust system: An example of induced subduction initiation along a plate boundary transform: GSA Bulletin, <https://doi.org/10.1130/B35752.1>.

Supplemental Material

1. Detrital Zircon U-Pb Geochronology Methods and References
2. $^{40}\text{Ar}/^{39}\text{Ar}$ Geochronology Methods and References
3. Figure S4 caption
4. Stratigraphic descriptions for the Last Chance Range and Jackass Flat.

Figure S1. Age Probability Distribution Diagram of Sanidine $^{40}\text{Ar}/^{39}\text{Ar}$ Ages.

Figure S2. $^{40}\text{Ar}/^{39}\text{Ar}$ Step-heating Age Spectrum for Basalt Groundmass

Figure S3. Geologic Map of Jackass Flats, Inyo County, California (Color version)

Figure S4. Stratigraphic Correlation of the White-Inyo and Death Valley facies

Table S1. Sanidine $^{40}\text{Ar}/^{39}\text{Ar}$ Geochronologic Data

Table S2. Basalt Groundmass $^{40}\text{Ar}/^{39}\text{Ar}$ Geochronologic Data

Table S3. Zircon U-Pb Geochronologic Data

1. DETRITAL ZIRCON U-Pb GEOCHRONOLOGY METHODS

Samples analyzed at UT Austin

Rock samples were crushed and sent to GeoSep Services for zircon separation by conventional techniques. Zircons were poured onto double-sided tape, mounted in epoxy and polished in-house at UNR. Cathodoluminescence (CL) images of the mounts were collected to guide laser spot analyses.

The primary standard used was GJ1 (Jackson et al., 2004) and secondary standards include 91500 ($^{238}\text{U}/^{206}\text{Pb}$ age of 1065 Ma), and Plesovice ($^{238}\text{U}/^{206}\text{Pb}$ age of 337 Ma). Laser spot size was 30 micron for all magmatic samples. Laser energy was set to 4 mJ, with 300 analysis shots at 10 Hz. The fluence was set at 3.88 J/cm².

Samples analyzed at the Institute for Tibetan Plateau Research

Samples were crushed using conventional jaw crusher and disk mill techniques, and zircons were separated using the Frantz magnetic separator and a standard heavy liquids protocol.

The zircon standards used were Plesovice and glass reference material NIST SRM 612 (Pearce et al., 1997). The first 15 s with the laser-off mode were used to collect the background values, and the following 40 s with the laser-on mode were employed to measure the peak intensities of the ablated material. A 25 micron laser spot size was used on all grains.

For zircon grains that are older than 1.0 Ga, $^{206}\text{Pb}/^{207}\text{Pb}$ age is reported. $^{206}\text{Pb}/^{207}\text{Pb}$ ages are preferred for older grains because the age uncertainty decreases with age for $^{206}\text{Pb}/^{207}\text{Pb}$, and increases for $^{206}\text{Pb}/^{238}\text{U}$. The uncertainty of young $^{206}\text{Pb}/^{207}\text{Pb}$ ages is due to the low abundance of ^{206}Pb and difficulty in measuring ^{207}Pb (Gehrels et al., 2008). $^{206}\text{Pb}/^{207}\text{Pb}$ ages (>1.0 Ga) that are >30% discordant are filtered out of the data set. Likewise, $^{206}\text{Pb}/^{238}\text{U}$ ages (<1.0 Ga) that are >30% discordant and have >10% error are excluded.

REFERENCES CITED

- Gehrels, G., Valencia, V.A., and Ruiz, J., 2008, Enhanced precision, accuracy, efficiency, and spatial resolution of U-Pb ages by laser ablation–multicollector–inductively coupled plasma mass spectrometry: *Geochemistry Geophysics Geosystems*, v. 9, Q03017, <https://doi.org/10.1029/2007GC001805>.
- Jackson, S.E., Pearson, N.J., Griffin, W.L., and Belousova, E.A., 2004, The application of laser ablation-inductively coupled plasma-mass spectrometry to in situ U-Pb zircon geochronology: *Chemical Geology*, v. 211, p. 47–69, <https://doi.org/10.1016/j.chemgeo.2004.06.017>.
- Pearce, N.J., Perkins, W.T., Westgate, J.A., Gorton, M.P., Jackson, S.E., Neal, C.R., and Chenery, S.P., 1997, A compilation of new and published major and trace element data for NIST SRM 610 and NIST SRM 612 glass reference materials: *Geostandards Newsletter*, v. 21, p. 115–144, <https://doi.org/10.1111/j.1751-908X.1997.tb00538.x>.

2. $^{40}\text{Ar}/^{39}\text{Ar}$ GEOCHRONOLOGY METHODS

Near-horizontal basalt flows within the Last Chance Range were dated to determine the extent of post-eruption tilting of the range. $^{40}\text{Ar}/^{39}\text{Ar}$ geochronology of basalt groundmass and sanidine from rhyolite tuff was conducted at the Nevada Isotope Geochronology Laboratory at the University of Nevada, Las Vegas.

The basalt groundmass experienced excess Ar complications, but an inverse isochron diagram provides an age of 5.528 ± 0.044 Ma with the $^{40}\text{Ar}/^{36}\text{Ar}$ intercept at 347. This is in agreement with a previously published K-Ar whole-rock age of 5.5 ± 0.2 Ma (Miller and Wrucke, 1995). Analysis of sanidine from the underlying rhyolite tuff return an age of 5.51 ± 0.03 Ma for 9 grains out of 14. These ages overlap within uncertainty, therefore we assign a general age of 5.51 Ma for the paleohorizontal marker.

LC 12B – Lapilli Tuff (sanidine) – 37.194371 N, -117.660864 W

LC 12A – Basalt (groundmass)–37.194371 N, -117.660864 W

Nevada Isotope Geochronology Laboratory - Description and Procedures

Samples analyzed by the $^{40}\text{Ar}/^{39}\text{Ar}$ method at the University of Nevada Las Vegas were wrapped in Al foil and stacked in 6 mm inside diameter sealed fused silica tubes. Individual packets averaged 2 mm thick and neutron fluence monitors (FC-2, Fish Canyon Tuff sanidine) were placed every 5–10 mm along the tube. Synthetic K-glass and optical grade CaF_2 were included in the irradiation packages to monitor neutron induced argon interferences from K and Ca. Loaded tubes were packed in an Al container for irradiation. Samples irradiated at the U. S. Geological Survey TRIGA Reactor, Denver, CO were in-core for 7 h in the 1 MW TRIGA type reactor. Correction factors for interfering neutron reactions on K and Ca were determined by repeated analysis of K-glass and CaF_2 fragments. Measured $(^{40}\text{Ar}/^{39}\text{Ar})_{\text{K}}$ values were $3.22 (\pm 6.64\%) \times 10^{-2}$. Ca correction factors were $(^{36}\text{Ar}/^{37}\text{Ar})_{\text{Ca}} = 2.33 (\pm 0.83\%) \times 10^{-4}$ and $(^{39}\text{Ar}/^{37}\text{Ar})_{\text{Ca}} = 6.82 (\pm 0.65\%) \times 10^{-4}$. J factors were determined by fusion of 5–6 individual crystals of neutron fluence monitors which gave reproducibility's of 0.09% to 0.12% at each standard position. Variation in neutron fluence along the 100 mm length of the irradiation tubes was <4%. Matlab curve fit was used to determine J and uncertainty in J at each standard position. No significant neutron fluence gradients were present within individual packets of crystals as indicated by the excellent reproducibility of the single crystal fluence monitor fusions.

Irradiated FC-2 sanidine standards together with CaF_2 and K-glass fragments were placed in a Cu sample tray in a high vacuum extraction line and were fused using a 20 W CO_2 laser. Sample viewing during laser fusion was by a video camera system and positioning was via a motorized sample stage. Samples analyzed by the furnace step heating method utilized a double vacuum resistance furnace similar to the Staudacher et al. (1978) design. Reactive gases were removed by three GP-50 SAES getters prior to being admitted to a MAP 215–50 mass spectrometer by expansion. The relative volumes of the extraction line and mass spectrometer allow 80% of the gas to be admitted to the mass spectrometer for laser fusion analyses and 76% for furnace heating analyses. Peak intensities were measured using a Balzers electron multiplier by peak hopping through 7 cycles; initial peak heights were determined by linear regression to the time of gas admission. Mass spectrometer discrimination and sensitivity was monitored by repeated analysis of atmospheric argon aliquots from an online pipette system. Measured $^{40}\text{Ar}/^{36}\text{Ar}$ ratios were $286.52 \pm 0.07\%$ during this work, thus a discrimination correction of

1.0313 (4 AMU) was applied to measured isotope ratios. The sensitivity of the mass spectrometer was $\sim 6 \times 10^{-17}$ mol mV^{-1} with the multiplier operated at a gain of 36 over the Faraday. Line blanks averaged 2.52 mV for mass 40 and 0.01 mV for mass 36 for laser fusion analyses and 26.83 mV for mass 40 and 0.09 mV for mass 36 for furnace heating analyses. Discrimination, sensitivity, and blanks were relatively constant over the period of data collection. Computer automated operation of the sample stage, laser, extraction line and mass spectrometer as well as final data reduction and age calculations were done using LabSPEC software written by B. Idleman (Lehigh University). An age of 28.02 Ma (Renne et al., 1998) was used for the Fish Canyon Tuff sanidine fluence monitor in calculating ages for samples.

For $^{40}\text{Ar}/^{39}\text{Ar}$ analyses a plateau segment consists of 3 or more contiguous gas fractions having analytically indistinguishable ages (i.e., all plateau steps overlap in age at $\pm 2\sigma$ analytical error) and comprising a significant portion of the total gas released (typically $>50\%$). Total gas (integrated) ages are calculated by weighting by the amount of ^{39}Ar released, whereas plateau ages are weighted by the inverse of the variance. For each sample inverse isochron diagrams are examined to check for the effects of excess argon. Reliable isochrons are based on the MSWD criteria of Wendt and Carl (1991) and, as for plateaus, must comprise contiguous steps and a significant fraction of the total gas released. All analytical data are reported at the confidence level of 1σ (standard deviation).

REFERENCES CITED

- Miller, R.J., and Wrucke, C.T., 1995, Age, chemistry, and geologic implications of Tertiary volcanic rocks in the Last Chance Range and part of the Saline Range, Northern Death Valley region, California: *Isochron-West*, v. 62, p. 30–36.
- Renne, P.R., Swisher, C.C., Deino, A.L., Karner, D.B., Owens, T.L., and DePaolo, D.J., 1998, Intercalibration of standards, absolute ages and uncertainties in $^{40}\text{Ar}/^{39}\text{Ar}$ dating: *Chemical Geology*, v. 145, p. 117–152, [https://doi.org/10.1016/S0009-2541\(97\)00159-9](https://doi.org/10.1016/S0009-2541(97)00159-9).
- Staudacher, T.H., Jessberger, E.K., Dorflinger, D., and Kiko, J., 1978, A refined ultrahigh-vacuum furnace for rare gas analysis: *Journal of Physics. E, Scientific Instruments*, v. 11, p. 781–784, <https://doi.org/10.1088/0022-3735/11/8/019>.
- Wendt, I., and Carl, C., 1991, The statistical distribution of the mean squared weighted deviation: *Chemical Geology*, v. 86, p. 275–285.

3. FIGURE S4 CAPTION

Comparison of the Neoproterozoic-Cambrian strata of the White-Inyo facies and the Death Valley facies (modified from Nelson (1976 and Chapman et al. (2015)). Biostratigraphic correlation of facies by Nelson (1976) is shown with the gray dashed line. The stratigraphic location of detrital zircon samples compiled in this study are shown by colored stars. 1—Maclean et al., 2009; 2—Schoenborn et al., 2012; 3—Gehrels and Pecha, 2014. See text Table 1 for detailed sample information and references.

REFERENCES CITED

- Chapman, A.D., Ernst, W.G., Gottlieb, E., Powerman, V., and Metzger, E.P., 2015, Detrital zircon geochronology of Neoproterozoic–Lower Cambrian passive-margin strata of the White-Inyo Range, east-central California: Implications for the Mojave–Snow Lake fault hypothesis: *Geological Society of America Bulletin*, v. 127, p. 926–944, <https://doi.org/10.1130/B31142.1>.
- Nelson, C.A., 1976, Late Precambrian–early Cambrian stratigraphic and faunal succession of eastern California and the Precambrian-Cambrian boundary, *in* Moore, J.N., and Fritsche, A.E., eds., *Depositional Environments of Lower Paleozoic Rocks in the White-Inyo Mountains, Inyo County, California*: Society of Economic Paleontologists and Mineralogists, Pacific Section, Pacific Coast Paleogeography Field Guide 1, p. 31–42.

4. STRATIGRAPHIC DESCRIPTIONS FOR THE LAST CHANCE RANGE AND JACKASS FLAT

Last Chance Range Stratigraphy

Paleozoic lithologic units

The oldest lithologic unit in the Last Chance Range is the Neoproterozoic-Cambrian Wood Canyon Formation (Fig. 4). This unit is characterized by thin- to medium bedded sandstone with minor shale and siltstone beds and a distinct limestone member separating the lower and upper clastic members. The base of the ~400-m-thick Wood Canyon Formation is not observed in the Last Chance Range. The upper contact with the Zabriskie Quartzite is gradational.

The Cambrian Zabriskie Quartzite is a distinct, ~300-m-thick massive quartz arenite with the lower section comprised of medium-bedded cross-bedded sandstone. The upper contact with Carrara Formation is gradational over ~10 m.

The Carrara Formation is an ~500-m-thick section of thin-to-medium bedded silt- and sandstone grading into a middle blue-green limestone member (Fig. 4). The upper tan limestone member is absent due to faulting in the northern map area (Fig. 5). A distinct white quartz sandstone and dark brown limestone are useful marker beds within the lower Carrara Formation. The white sandstone is the younger, stratigraphically higher unit. The unit is typically overturned in the northern Last Chance Range as indicated by cross bedding. The upper contact with the Bonanza King Formation is sharp.

The middle Cambrian Bonanza King Formation is a cliff-forming, thick-bedded dolomite with infrequent buff-white limestone marker beds. Bed composition and texture varies significantly from marl to mottled dolomite, thin-bedded dolomite and shale, and massive limestone. The alternating white and grey beds form useful markers. The upper contact with the Dunderberg Shale member of the Nopah Formation is sharp.

The Dunderberg Shale, a classic marker bed across California and Nevada, is an ~50-m-thick shale with chert ribbons and a thin upper limestone bed. The thickness of the Dunderberg Shale varies across the Last Chance Range and is tectonically thinned in some locations. The overlying member of the upper Cambrian Nopah Formation is a 450 m-thick, medium bedded limestone. The interbedded siltstones and marls grade up-section into dominantly limestone with an upper section of dolomite. The upper contact with the Pogonip Group is gradational and marked by the appearance of distinct chert nodules and limestone of the lower Pogonip Group.

The Ordovician Pogonip Group consists of the lower member, an ~900-m-thick medium bedded limestone with interbedded shale that grades up-section into massive limestone, and the Antelope Valley Limestone member, an ~450-m-thick, thin-bedded limestone with thin red siltstone and occasional marl beds (Fig. 4). This unit is distinguished from the lower Pogonip member by the thin red siltstone beds.

The overlying Ordovician Eureka Quartzite is another classic marker bed of California and Nevada (Fig. 4). In the Last Chance Range, an ~35-m-thick section of distinct pure white quartz sandstone with medium to massive bedding and occasional cross stratification is observed. The contact with the overlying Ely Springs Dolomite is sharp.

The upper Ordovician Ely Springs Dolomite is an ~300-m-thick, thin-bedded to massive fossiliferous dolomite with abundant chert nodules in the lower part of the section (Fig. 4). The upper contact is not observed in the Hanging Rock Canyon quadrangle.

The Silurian-Devonian Hidden Valley Dolomite had been placed atop the Ely Springs Dolomite by a fault (Fig. 4). The ~100-m-thick section of the Hidden Valley Dolomite consists of thin-bedded shale and dolomite with occasional medium marl beds. In the northeastern Last Chance Range, the Hidden Valley Dolomite is exposed as extensional klippen in the hanging wall of a low-angle fault over the Ely Springs Dolomite (Fig. 5). Tight meter-scale folds are abundant in the hanging wall adjacent to the fault. The upper contact of the unit is not observed.

The lower plate stratigraphy of the Last Chance thrust system is often difficult to distinguish due to extensive deformation (Fig. 4). The Devonian Lost Burro Dolomite is an ~20-50-m-thick, massive dolomite exposed sporadically in the central Last Chance Range (Fig. 5). The dolomitic composition of this unit distinguishes it from the overlying Mississippian Perdido Formation.

The Mississippian Perdido Formation is a distinct footwall unit, comprised primarily of a sequence of shale, thin-bedded siltstone and cherty pebble conglomerate with interbeds of massive limestone near the top of the formation (Fig. 4). Foliation is commonly parallel to original bedding. In some locations, the pebble conglomerate is ductilely deformed to form an L-S tectonite. Unit thickness is variable owing to pervasive deformation, but it is ~55 m thick. The contact with the overlying Rest Spring Shale is gradational.

The Mississippian Rest Spring Shale is a locally phyllitic shale displaying pervasive internal deformation (Fig. 4). This unit is commonly folded and exhibits a strong foliation parallel to original bedding. Scattered thin white- to red-colored quartz sandstone beds are common. Rest Spring Shale is the youngest Paleozoic unit in the Last Chance Range and forms the stratigraphically highest footwall unit of the Last Chance thrust. The true stratigraphic thickness is unknown due to tectonic thinning, but the exposed thickness is ~30 m.

Jackass Flats Stratigraphy

The Neoproterozoic-Cambrian stratigraphy of the White-Inyo Mountains is lithologically distinct from that of the Last Chance Range to the east. The lowest exposed unit is the Neoproterozoic Wyman Formation (Fig. 8), which is a >2,700 m-thick succession of thin-bedded argillite, fine-grained quartzite, and siltstone interbedded with oolitic limestone lenses. The basal contact of the Wyman Formation is not exposed.

Unconformably overlying the Wyman Formation is the ~600-m-thick Reed Dolomite, which is subdivided into three members at Jackass Flats (Fig. 8). The lower member is a coarse-grained oolitic dolomite overlain by a >200-m-thick lens of quartzite and carbonaceous sandstone of the Hines Tongue Member. The upper member of the Reed Dolomite is a fine-grained dolomite. The contact with the overlying Deep Springs Formation is gradational.

The Deep Springs Formation is comprised of a >450-m-thick sequence divided into a lower fine-grained limestone, a middle member of quartzite overlain by interbedded limestone, shale and siltstone, and an upper member of quartz sandstone and siltstone capped by a massive dolomite unit (Fig. 8). The contact with the overlying Campito Formation is sharp.

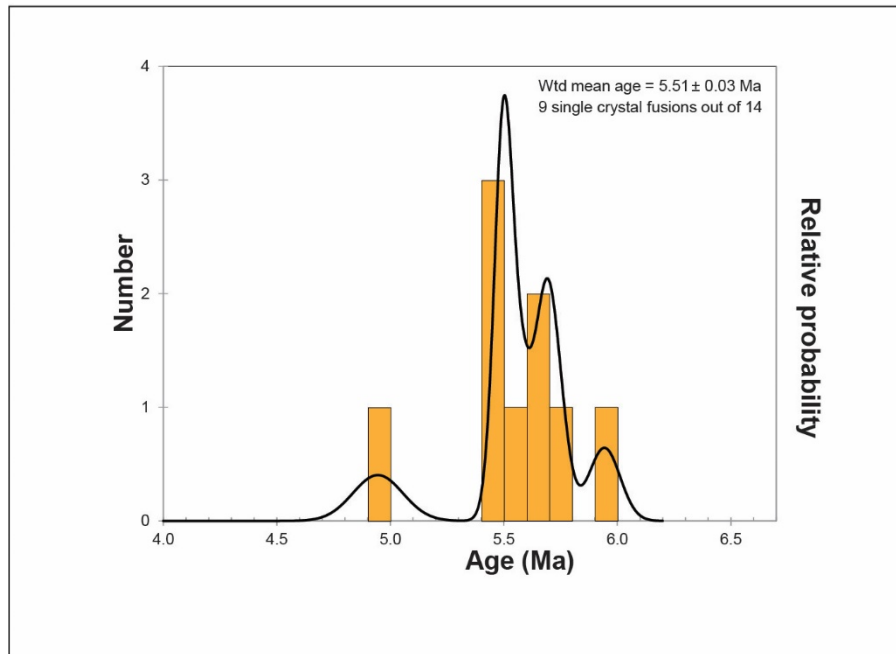
The Campito Formation consists of >1000 m of quartzite, siltstone, and shale (Fig. 8). The base of the formation is comprised of the Andrews Mountain Member, a >700-m-thick stack of massive quartz sandstone with interbedded siltstone and shale. The Andrews Mountain Member is overlain by shale with coarser-grained siltstone and sandstone of the Montenegro Member, which consists of grey shale with coarser grained interbeds of siltstone and sandstone.

Overlying the Campito Formation is the Poleta Formation (Fig. 8), which consists of >350 m of massive-to-thick bedded limestone, thin-bedded quartz sandstone and siltstone. The contact with the overlying Harkless Formation is abrupt.

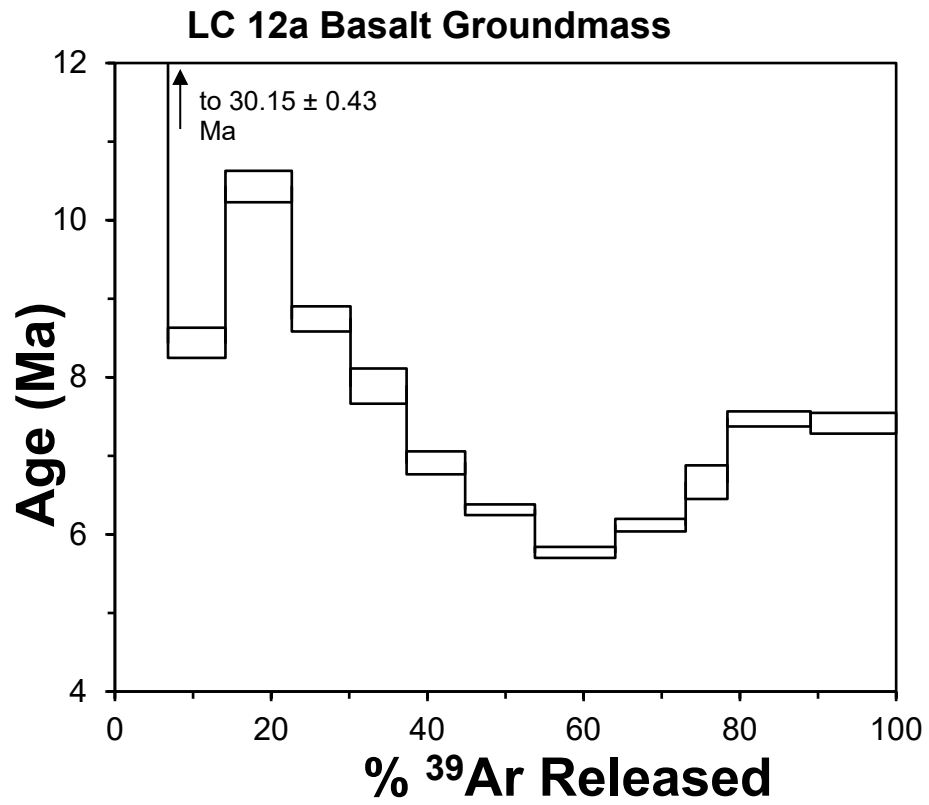
The ~600-m-thick Harkless Formation is composed of phyllitic shale with interbeds of quartz sandstone, siltstone and distinct limestone marker beds (Fig. 8). The Harkless Formation grades into the massive quartzite of the >250-m-thick Saline Valley Formation. The upper contact of the Saline Valley Formation with the overlying Mule Spring Limestone is sharp.

The Mule Spring Limestone is an ~300-m-thick section of bedded limestone (Fig. 8). A sharp upper contact with the Monola Formation leads into ~380 m of shale and siltstone, massive limestone, and thin-bedded fine grained limestone interbedded with siltstone and shale. The overlying Bonanza King Formation is the oldest unit of an upper Cambrian-Ordovician carbonate succession that is continuous across the White-Inyo Mountains and Death Valley region.

Sample LC 12b

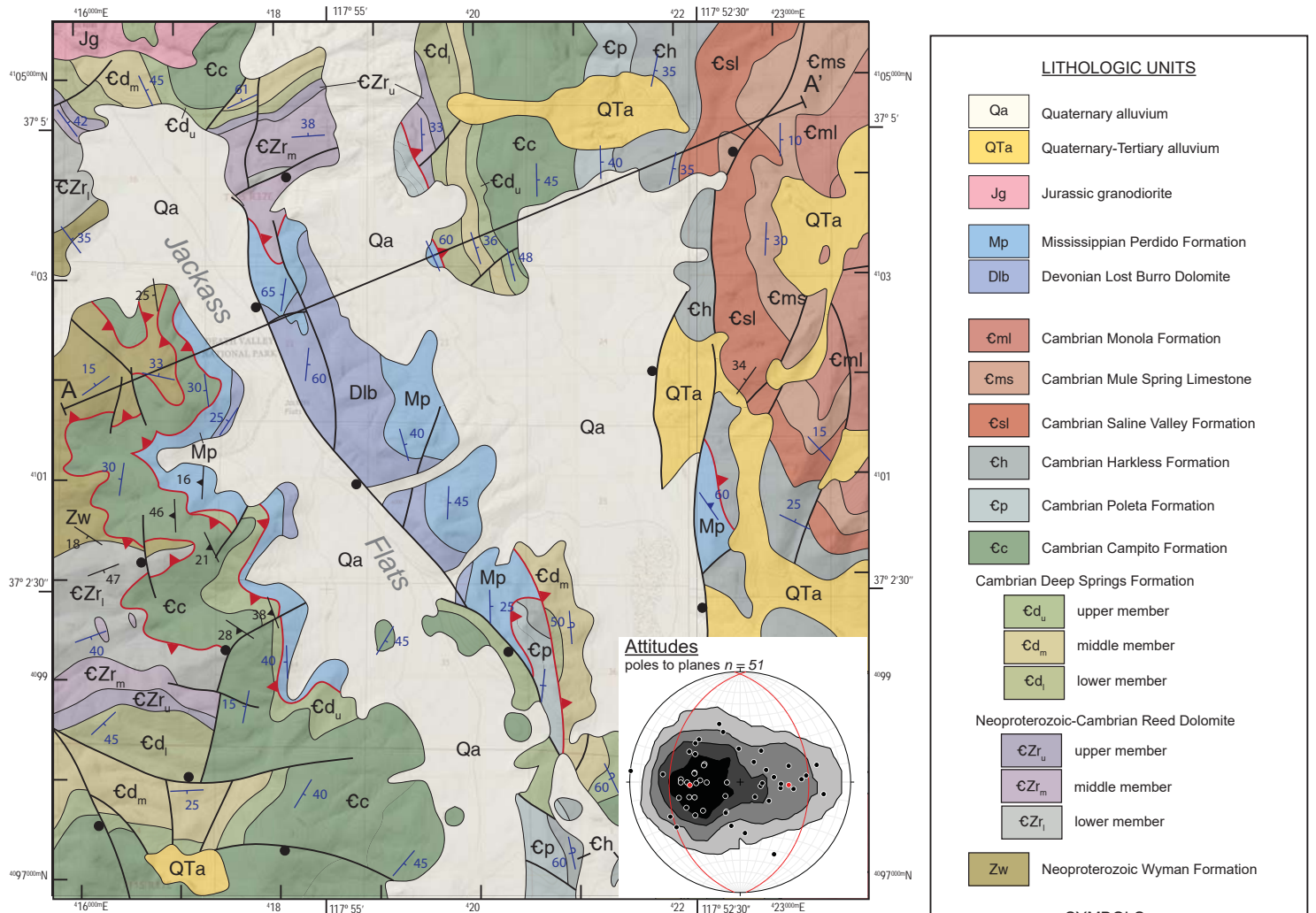


Supplementary Figure 1: Age probability distribution diagram of sanidine $^{40}\text{Ar}/^{36}\text{Ar}$ ages.

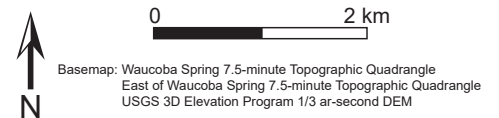
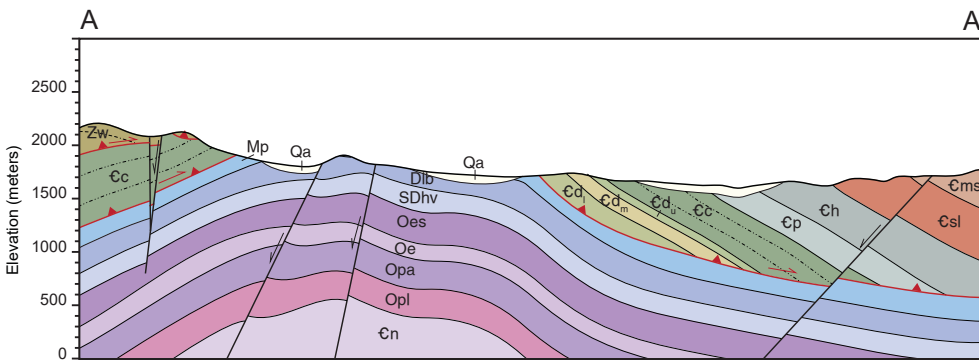


Supplementary Figure 2: ⁴⁰Ar/³⁹Ar Step-heating Age Spectrum for Basalt Groundmass

A. Geologic Map of Jackass Flat, Inyo Mountains, California



B. Cross Section of Jackass Flat



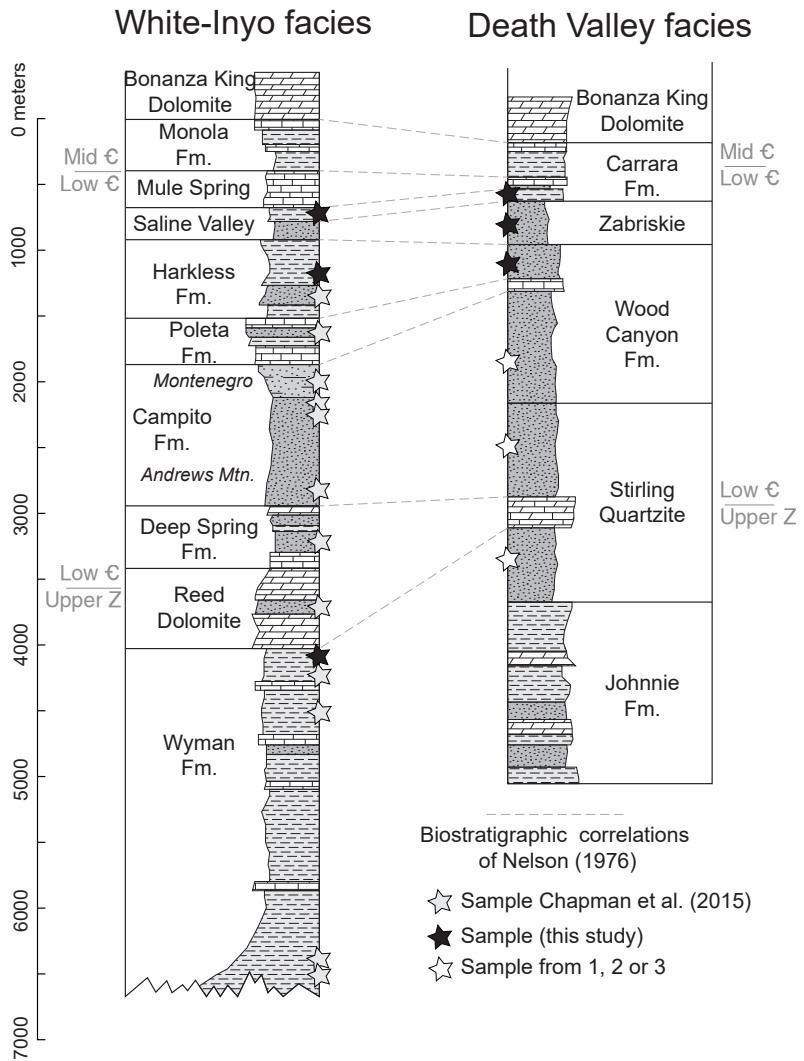


Figure 10